A Parametric Study on the Application of Finlets for Trailing Edge Noise Reduction of a Flat Plate

Felix Gstrein*, Bin Zang† and Mahdi Azarpeyvand‡
Faculty of Engineering, University of Bristol, United Kingdom, BS8 1TR

An experimental investigation on the use of specific surface treatments, called finlets, was performed to achieve noise reduction at the trailing edge of a flat plate. For the first time, comprehensive measurements, such as surface static and dynamic pressure measurements, carried out in the space between the finlets, are presented. These provide further understanding of the flow dynamics and their correlation with the noise reduction at the trailing edge. Moreover, with an ultimate goal of effective and efficient application of finlets in commercial aviation, configurable parameters such as treatment position, finlet spacing and finlet profile shape were considered and their effects on the flow physics and noise reduction examined. In doing so, the effects of finlet application on turbulent structures in the boundary layer were investigated. The results show that when the turbulent structures were allowed to be convected some distance after leaving the finlets, they were less effective in noise production through trailing-edge scattering. Furthermore, it was observed that a variation of the finlet profile shape can improve the efficiency of the treatment in reducing the surface pressure fluctuation power spectral density, but at the same time is likely to lead to an increase of the finlet self-noise.

I. Nomenclature

L	=	flat plate length
s	=	flat plate span
d	=	pinhole diameter
d^+	=	dimensionless pinhole diameter
h_F	=	finlet height
l_F	=	finlet length
p_F	=	finlet position
s_F	=	finlet spacing
C_p	=	pressure coefficient
M_∞	=	incident Mach number
p_0	=	reference pressure
Re_L	=	length-based Reynolds number
S_{pp}	=	power spectral density of the far-field sound pressure
U_∞	=	flow speed
u_τ	=	friction velocity
u	=	velocity distribution in x-direction
(x, y, z)	=	coordinate system set at the flat plate leading edge
(x_F, y_F, z_F)	=	coordinate system set at the finlet leading edge
α	=	angle of attack
δ	=	boundary layer thickness
Λ_z	=	spanwise correlation length
ν	=	kinematic viscosity of the flow medium
Φ_{pp}	=	power spectral density of surface pressure fluctuations

*PhD Researcher, Mechanical Engineering, felix.gstrein@bristol.ac.uk.
†Research Associate, Aerospace Engineering, nick.zang@bristol.ac.uk.
‡Professor of Aerodynamics and Aeroacoustics, m.azarpeyvand@bristol.ac.uk.

II. Introduction

Noise pollution caused by aviation is constantly growing due to expanding capacities in airports and flight routes. Thus, the European Union started a number of initiatives to tackle this issue in recent years. In 2011, the European Commmission [1] explicitly set out a future target to reduce the noise emission by 65% compared to the state of the year 2000. Since then, several research and development projects have been initiated dealing with novel technologies to mitigate the high-level noise emission by commercial aerial vehicles. Among the various noise sources, trailing edge noise has been identified as one of the primary contributors to the overall sound generated by turbines and air-frames [2]. In the context of this study, surface treatments known as finlets, protruding from the surface of an object immersed in a flow, are applied and investigated as an innovative passive strategy to reduce trailing edge noise.

Noise is generated when eddies within a turbulent boundary layer are convected past the trailing edge. The fluctuations of the surface pressure, originating from these turbulent structures, are scattered by the presence of a solid trailing edge boundary and subsequently propagated as far-field noise. According to Amiet's Theory [3] on trailing edge noise generated by a flat plate, the far-field sound pressure power spectral density at the center line, S_{pp}, mainly depends on the surface pressure fluctuation power spectral density, Φ_{pp}, and the lateral correlation length Λ_z of boundary layer turbulence structures at the trailing edge. The pressure fluctuation power spectral density and correlation length are both frequency dependent. In his paper on the silent flight of owls, Lilley [4] argued that the downy structures on the wings of certain owls help reduce high-frequency pressure fluctuations above 2000 Hz. He attributed this phenomenon to a shift of the natural cut-off frequency due to dissipation of small-scale eddies in the boudary layer toward lower frequencies, triggered by the absorption of energy by the downy structures. His hypothesis was experimentally confirmed by Clark et al. [5]. On the basis of this research, Clark et al. [6, 7] introduced novel surface treatments, termed "finlets", which were intended to resemble the surface characteristics of owl wings. Though originally placed at the trailing edge of a DU96-W180 airfoil, Clark et al. observed beneficial effects on the reduction of noise above frequencies of 3000 Hz when the finlets were moved away from the trailing edge, toward the leading edge of the airfoil. Later, Afshari et al. [8, 9] applied similar finlets on a flat plate some distance upstream of the trailing edge and observed a notable reduction of surface pressure fluctuations. With reference to Amiet's theory, they identified the finlet spacing s_F, i.e. the spanwise distance of the finlets to each other, as a critical parameter for efficient noise reduction. Furthermore, Afshari et al. [9] concluded that with an optimal spacing of approximately $0.07 \cdot \delta$, with δ being the boundary layer thickness on the untreated flat plate, the strongest reduction at high frequencies from 1000 Hz to 10 000 Hz is achieved, while retaining a similar noise level as the untreated flat plate in the low-frequency range from 50 Hz to 500 Hz. As a variant of finlets, Afshari et al. [10] also introduced three-dimensional surface treatments for trailing edge noise reduction, showing results similar to those for the conventional finlets, but with an increased efficiency in reducing trailing edge noise. The related treatments consisted of similar finlets, except that they were arranged in staggered configurations. Recently, numerical studies on the application of finlets were performed by Bodling and Sharma [11, 12]. Thereby, the flow over a NACA 0012 airfoil, treated with finlets slightly extending beyond the trailing edge, at 0° angle of attack and a Mach number of $M_\infty = 0.2$ was simulated using a wall-resolved Large Eddy Simulation (LES) approach. The authors attributed the capability of finlets to reduce noise partly to the lifting of eddies away from the trailing edge, therefore decreasing the scattering of sound.

Inspired by the previous work demonstrating the effectiveness of finlets on noise reduction, the present study aims to further enhance the understanding of the noise reduction mechanisms of finlets applied to a flat plate through detailed experimental measurements of surface pressure fluctuations and other flow characteristics between the finlets. The use of the flat plate helps to elucidate the underlying flow physics caused by finlets without geometric complications, and thus will serve as a building block toward the employment of such passive surface treatments to airfoils and high-lift devices. The structure of this work is as follows: The experimental set-up for the measurement procedures is described in Section III. Subsequently, in Section IV the analyzed data from the experiments are presented and discussed. Firstly, the choice of the finlet position is explained, which was then used for the investigation of finlet spacing variations. Finally, the role of the profile shape is examined. Section V contains the conclusions from the results and explanations of intended future research.

III. Experimental Set-up

A. Treatment Designs

The design of the conventional finlets used in this study follows closely that of Afshari et al. [9] and Clark et al. [7]. To give an idea of their application, a schematic of the experimental set-up with the flat plate, the nozzle and finlets

including the reference coordinate system is shown in Fig. 1. The support structure has been omitted to allow a better view on the flat plate with the treatment.

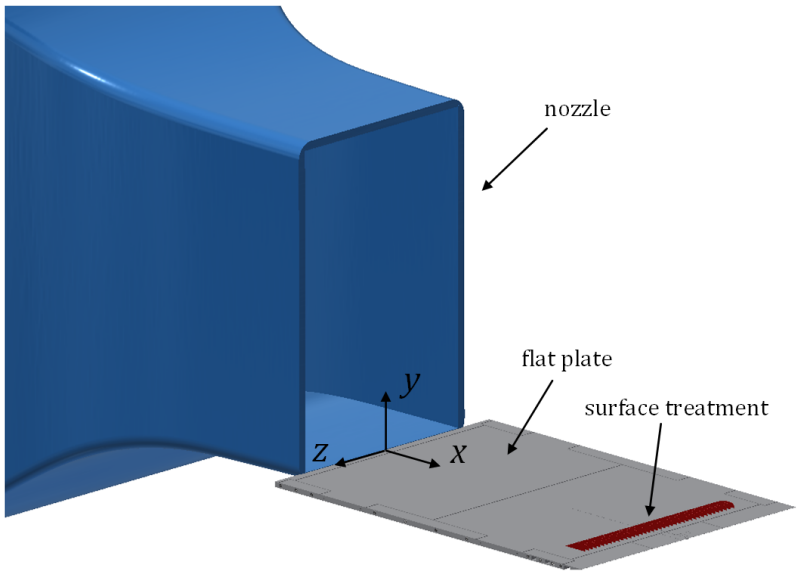

Fig. 1 Schematic of the set-up with finlet treatment applied upstream of the flat plate trailing edge.

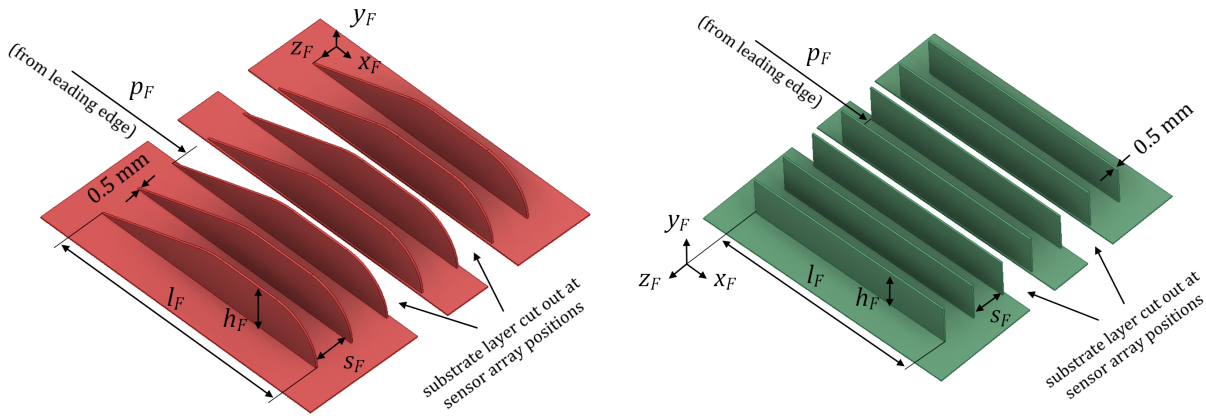

Fig. 2 Finlet treatments applied on the flat plate's upper surface: a) conventional and b) rectangular profile.

Finlet parameters and installation details are illustrated in Fig. 2. At the conventional finlet leading edge, the profile follows the shape of the curve describing the turbulent boundary layer thickness on a flat plate,

$$y = a \cdot x_F^{4/5}. \tag{1}$$

This allows the boundary layer flow to enter the treated area smoothly without undergoing sudden changes. In Eq. (1) $x_F = x - p_F$ is the streamwise coordinate direction starting at the leading edge of the finlets, where x designates the corresponding reference coordinate in the streamwise direction starting at the flat plate's leading edge. The dimensionless parameter a describes the gradient of the finlet leading edge and is chosen such that the length of the tapered part is constant for all different finlet heights. This length is about 33 mm in the present study, and thus $a = 1.4775$ applies for a finlet height of 12 mm. The conventional finlet trailing edge is rounded with a radius equal to the profile height to

avoid sharp edges and thus sharp changes to the dynamics of the flow. In order to evaluate the role of the profile shape, the conventional treatments were compared with rectangular ones.

All finlet treatments used are 0.5 mm thick and supported by a flat, 0.3 mm substrate layer base holding the finlets upright in place. As shown in Fig. 2, the substrates were locally removed and finlets carefully aligned with the flow such that both the miniature microphone pinholes and the static pressure ports located within the gaps of the finlets remained uncovered during measurements. The parametric study includes variations of the finlet position, p_F, with respect to the leading (and thus also trailing) edge, i.e. the distance along the x-coordinate, and the finlet spacing, s_F. The finlet position was varied from $p_F = 0.5 \cdot L$ to $p_F = 0.935 \cdot L$, where L refers to the total length of the flat plate, and the finlet spacing from $s_F = 2\,\text{mm}$ to $s_F = 15\,\text{mm}$. In the case of $p_F = 0.935 \cdot L$, the finlets end flush with the trailing edge as in the studies of Clark et al. [6, 7].

B. Flat Plate and Instrumentation

The flat plate used in the experiments is an assembly of two aluminum plates with exchangeable trailing edge and leading edge parts, which are also machined out of aluminum. Measuring a total length of $L = 1000\,\text{mm}$ and a span of $s = 700\,\text{mm}$, the flat plate was mounted flush with the lower nozzle lip line, as shown in Fig. 1, to ensure a two-dimensional flow past a flat plate at the nozzle exit. Moreover, to achieve the desired turbulent boundary layer characteristics, the flow was tripped close to the leading edge with 80-grit sandpaper. The trailing edge is tapered with an angle of 12° and extends from a thickness of 0.3 mm at its end to the thickness of the plate, which is 13 mm.

A total number of 45 miniature microphones and 58 pressure taps were mounted beneath pinholes of diameter $d = 0.4\,\text{mm}$ to avoid surface pressure attenuation effects. The microphones are arranged along the x-coordinate axis with a constant interval of $0.006 \cdot L$ from $x/L = 0.834$ to $x/L = 0.996$, except for one omitted transducer at the transition from the main body to the interchangeable trailing edge part. For a velocity of $U_\infty = 15\,\text{m/s}$ (corresponding to a Reynolds number at the trailing edge $Re_L \approx 9.9 \cdot 10^5$), the dimensionless pinhole diameters $d^+ = d \cdot u_\tau/\nu$ can be roughly estimated as 17.4 and 17.1 at the first and last pressure transducer position respectively, seen from the flat plate leading edge. The symbols u_τ and ν, used to define d^+, designate the friction velocity and the kinematic viscosity of the flow medium respectively. These values lie within the range of $12.0 \leq d^+ \leq 18.0$ established by Gravante et al. [13], where spectral attenuation effects are non-existent. Furthermore, three spanwise rows of microphones were mounted at $x/L = 0.96$, 0.972 and 0.984 with their separation distances determined using an exponential formula similar to the approach used by Afshari et al. [9]. Such an approach is essential to obtain distinct microphone spacing intervals and hence facilitating the spanwise correlation length calculation. Knowles FG-23329-P07 dynamic pressure transducers were used as the miniature microphones because of their good frequency response within 0.1 kHz–10 kHz and small physical size.

C. Aeroacoustic Facility and Data Acquisition

The experiments were conducted in the aeroacoustic facility of the University of Bristol, a temperature-controlled closed-circuit wind tunnel. The nozzle used for the experiments has an opening section of 500 mm width and 775 mm height, which allows a maximum reachable flow speed of 40 m/s. The open jet test section is fully anechoic above 160 Hz, as determined in [14]. During the tests, different free stream velocities were considered such that the Reynolds number determined at the trailing edge, Re_L, varied between $9.9 \cdot 10^5$ and $1.3 \cdot 10^6$. Static pressure data from the pressure taps were processed by a Chell μDAQ-32DTC Smart Pressure Scanner. The pressure information was transferred to the scanner via polyurethane tubing of about 1 m length and sampled with 1000 Hz for 60 s. Velocity measurements were carried out using Dantec constant temperature anemometry (CTA) hot-wire boundary layer probes of type 55P15. The probes were operated by a Dantec Streamline Pro system with a CTA91C10 module and calibrated using a Dantec 54H10 calibrator. Recordings were performed together with dynamic surface pressure messurements at a sampling frequency of 2^{15} Hz for 62 s. To obtain data related to pressure only (i.e. decoupled from velocity measurements), the sampling duration was increased to 70 s. Note that the hot-wire anemometry and surface pressure measurements in this case were performed separately, to avoid any obstruction of the flow by the hot-wire and its mounting traverse. The dynamic pressure transducers were calibrated using a G.R.A.S. microphone of the type 40 PL. Both the in-situ FG microphone and the reference G.R.A.S. microphone were subjected to a white noise produced by a Visaton FRS 8 speaker, from which a transfer function could be obtained for each pressure transducer. This procedure was performed similar to the previous works [15–17]. The G.R.A.S. microphone itself was calibrated using the G.R.A.S. 42AA pistonphone. In the following discussions, dynamic surface pressure fluctuation data from the transducers are presented as power spectral density $\text{PSD} = 10 \cdot \log_{10}(\Phi_{pp}/p_0^2)$. Here, $p_0 = 20\,\mu\text{Pa}$ is the reference pressure and Φ_{pp} is determined using Welch's

method with a window size of 2^{12} samples and a Hamming window with 50 % overlap.

IV. Results and Discussion

A. Effect of Finlet Position

It has already been found by Clark et al. [7] that finlets influence boundary layer turbulence structures approaching the trailing edge instead of directly affecting the scattering mechanism. Hence, the question remains, whether the finlet efficiency increases when they are shifted toward the leading edge. Such a displacement would lead to a reduction of the Reynolds number Re_{p_F} at the start of the treated area, since the finlet position, p_F, is decreased. It might also give the modified flow patterns time to evolve into a favorable state. For the present efforts to understand the effects of finlet position, one selected treatment with height $h_F = 12\,\text{mm}$, spacing $s_F = 4\,\text{mm}$ and length $l_F = 65\,\text{mm}$ was applied at different positions p_F and tested at $Re_L = 9.9 \cdot 10^5$. The surface pressure fluctuation PSD for various finlet positions on the flat plate are shown in Fig. 3, for two pressure transducer positions at $x/c = 0.99$ and $x/c = 0.996$, most representative of the main area of interest at the trailing edge. To help better differentiate the various surface pressure fluctuation PSD, the results are presented in four subplots, each with a single pressure measurement for different finlet positions tested. The columns, i.e. Figs. 3a, c and 3b, d, represent the penultimate and the rearmost transducer position, respectively. The rows of Fig. 3 divide the data into different ranges for p_F. Relating to the baseline, i.e. the flat plate set-up without any treatments, the configuration with finlets applied generally shows promising results. A comparison of any treated configuration with the baseline shows a substantial reduction of Φ_{pp} at frequencies above 1000 Hz, accompanied by a less desirable increase at lower frequencies with a broadband peak between 100 Hz and

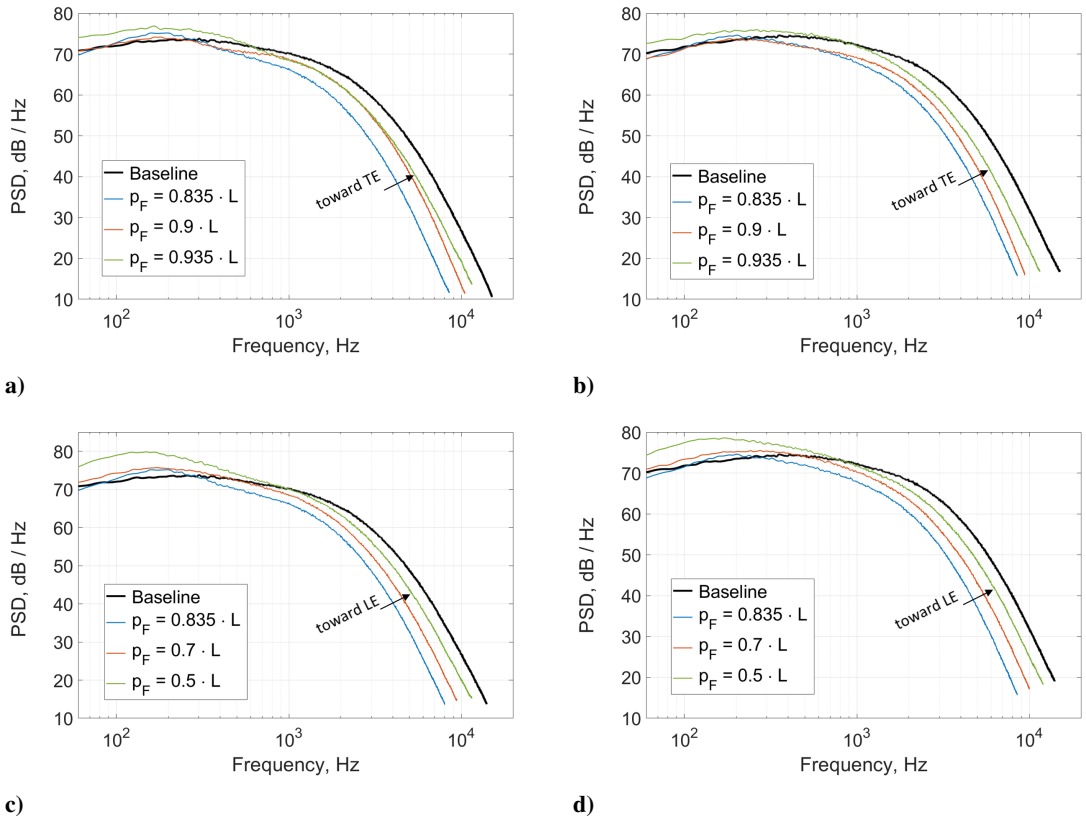

Fig. 3 Surface pressure fluctuation PSD for conventional finlets with $h_F = 12\,\text{mm}$, $s_F = 4\,\text{mm}$ and $l_F = 65\,\text{mm}$ applied at various positions at $Re_L = 9.9 \cdot 10^5$: a) $x/L = 0.99$, $p_F \geq 0.835 \cdot L$, b) $x/L = 0.996$, $p_F \geq 0.835 \cdot L$, c) $x/L = 0.99$, $p_F \leq 0.835 \cdot L$ and d) $x/L = 0.996$, $p_F \leq 0.835 \cdot L$.

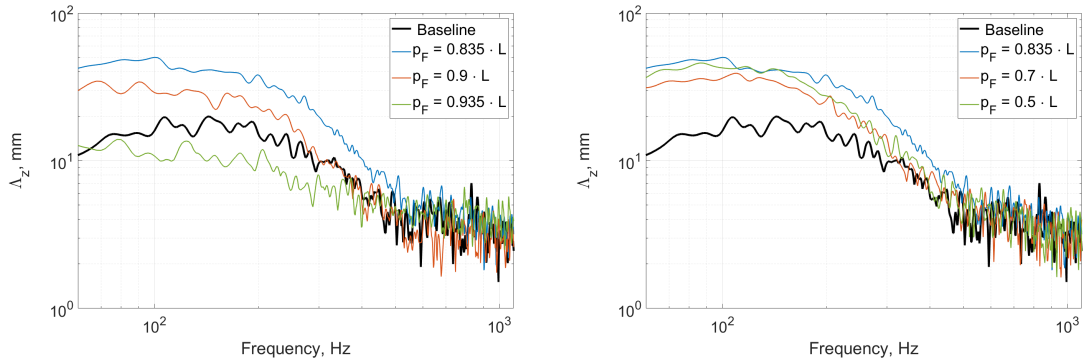

a) b)

Fig. 4 Spanwise correlation length of the boundary layer turbulence structures at $x/L = 0.984$ for conventional finlets with $h_F = 12\,\text{mm}$, $s_F = 4\,\text{mm}$, and $l_F = 65\,\text{mm}$ applied at various positions at $Re_L = 9.9 \cdot 10^5$: a) $p_F \geq 0.835 \cdot L$, b) $p_F \leq 0.835 \cdot L$.

300 Hz, arising from the treated configuration. As can be seen in any plot of Fig. 3, the peak surpasses the baseline only slightly, in most cases by less than 5 dB/Hz. The reduction at high frequencies on the other hand can exceed 20 dB/Hz, for instance at 8000 Hz for finlets applied at $p_F = 0.835 \cdot L$. Moreover, the data clearly indicate that an optimum position exists, which is located approximately at $p_F \approx 0.835 \cdot L$. As shown in the first row of Fig. 3, moving the finlets toward the trailing edge, i.e. increasing p_F from $p_F = 0.835 \cdot L$, led to an increase of Φ_{pp} across the majority of the frequency range considered. The same also holds true for decreasing p_F from $p_F = 0.835 \cdot L$, which is shown in the second row of Fig. 3. Further examination reveals that a reduction of more than 10 dB/Hz can be achieved for both microphone locations at frequencies around 8000 Hz when moving the finlet position from $p_F = 0.935 \cdot L$ to $p_F = 0.835 \cdot L$, suggesting that the finlet position is one of the key parameters to be considered in the finlet applications.

The spanwise correlation length, Λ_z, plotted against the signal frequency for each finlet position tested is shown in Fig. 4. The quantity reflects the spanwise length scale of the turbulence structures close to the trailing edge when the finlet treatment is positioned at various locations. For the treatment mounted flush with the trailing edge, the measurement positions of the laterally arranged sensors were located within the treated area. The minimum distance between the spanwise measurement positions exceeds a threshold such that no two sensors were spatially located within a single gap between two finlet walls for the finlet spacing $s_F = 4\,\text{mm}$. With the presence of finlets mounted flush to the trailing edge, the spanwise correlation length, represented by the graph for $p_F = 0.935 \cdot L$ in Fig. 4a, presumably measures the correlation between the distinct turbulent structures separated by the finlet walls. It can be seen that, for $p_F = 0.935 \cdot L$, Λ_z decreased compared to the baseline within the frequency range of 70 Hz to 500 Hz. This corroborates the assumption that large eddies are split into smaller ones divided by the finlet walls. However, it does not explain why the surface pressure fluctuation PSD in the aforementioned frequency range peaks for p_F considered. The reason for this could lie in the three-dimensional nature of the turbulent structures being channeled by the finlets. With the spanwise correlation length describing primarily the characteristics of the turbulence in spanwise (i.e. z-) direction, the low-frequency hump may be associated with the changes of the flow in the wall-normal (i.e. y-) direction instead.

For all p_F where the measurement position was located downstream of the treatment, Λ_z increased noticeably at frequencies lower than 500 Hz. From the result for $p_F = 0.935 \cdot L$ discussed in the previous paragraph, where the spanwise microphone transducers are separated by finlet walls, it can be inferred that the correlation of turbulence structures within the treatment decreases for other positions as well. The increase of Λ_z in the finlet wake, which can be observed for the tested finlet positions other than $p_F = 0.935 \cdot L$, suggests that the separate structures extended and merged again when leaving the spaces between the finlets. This probably eventually led to an increase in spanwise correlation length. According to the observations on Φ_{pp}, the mean-square pressure fluctuations, and thus the associated turbulent structures proceeding toward the trailing edge, then had a much lower intensity than upstream of the treatment.

B. Effect of Finlet Spacing

In their study [9], Afshari et al. identified two different noise reduction mechanisms related to finlet application upstream of the trailing edge. One was assumed to affect the flow similar to a backward facing step and the other one

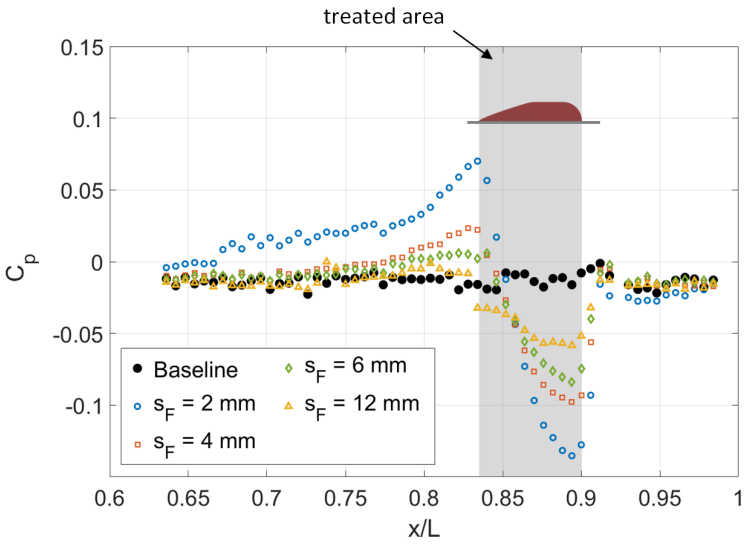

Fig. 5 Pressure coefficient for conventional finlets with $p_F = 0.835 \cdot L$, $h_F = 12\,\text{mm}$, $l_F = 65\,\text{mm}$ and various spacings at $Re_L = 9.9 \cdot 10^5$.

was explained to be a dissipation effect due to an increase of friction triggered by the additional surface area introduced by finlet walls, referred to as the "channeling" effect. The finlet spacing was identified as the factor determining which effect predominates. This section will discuss the implications of a variation of the finlet spacing, s_F, particularly the different effects on the small turbulent flow structures. Therefore, treatments of height $h_F = 12\,\text{mm}$, length $l_F = 65\,\text{mm}$ and different spacings, s_F, were placed at $p_F = 0.835 \cdot L$, which has been identified as efficient in reducing the near-field surface pressure fluctuation PSD. The Reynolds number was $Re_L = 9.9 \cdot 10^5$. Figure 5 shows the pressure coefficient, C_p, evaluated along the posterior third of the flat plate for the baseline and the flat plate treated with finlets with different spacings. Far upstream of each treatment, the static pressure was almost equal to or slightly elevated with reference to the baseline case. Directly upstream of the finlets, there is a pressure peak indicating that the flow was decelerated. The peak is preceded by an adverse pressure gradient, which starts at about the same position $x/L \approx 0.75$ for most of the treatments and grows as s_F decreases. For the smallest spacing $s_F = 2\,\text{mm}$, the pressure gradient sets in earlier at $x/L \approx 0.67$. Both the adverse pressure gradient and the pressure peak for this case are substantially larger than for all other s_F, suggesting that the treatment likely caused a different flow character. The large adverse pressure gradient is likely to cause a flow separation and the formation of eddies in front of the treatment. As can be seen, a spacing of $s_F = 12\,\text{mm}$ is almost large enough not to produce any adverse pressure effects. In all cases, the pressure increase is followed by a region with favorable pressure gradient within the treated area, highlighted with a gray band in Fig. 5. For the finlets with the smallest spacing, the pressure drop is substantially larger than for those with wider s_F. It is assumed that the flow was re-accelerated due to the presence of a favorable pressure gradient region for $s_F \geq 4\,\text{mm}$, whereas the flow is likely to be detached from the wall for $s_F = 2\,\text{mm}$. This corroborates the observations of Afshari et al. [9] that the two mechanisms, related to backward facing steps (i.e. small enough finlet spacing) and channeling respectively, exist. At the flow exit point, the static pressure shows a notably fast recovery, where C_p settles back to the baseline level within a distance of $x/L \approx 0.02$. Although this again means there is a strong pressure gradient, the fast recovery suggests that there is no extensive recirculation bubble in the finlet wake, such as it would be the case for a backward facing step. Indeed, it seems that the flow, if separated or deflected at the finlet leading edge, should have reattached already within the treated area instead, otherwise, the fluctuations in C_P should be more evident.

Figure 6 describes the development of the surface pressure fluctuation PSD along the center line of the plate from shortly after the flow entry point into the finlets to the trailing edge. Associated measurement positions are indicated next to the plots using a black line placed perpendicular to the boundary of the partial flat plate profile outlined in a schematic. Figure 6a shows the PSD 5 mm downstream of the treatment entry. Here, the energy exerted on the surface from low-frequency pressure fluctuations up to around 2000 Hz due to the application of finlets express themselves as an increase of Φ_{pp}. This complies with the notion that a large tubulence structure forms at the leading edge area of the finlets. Therefore, it can be inferred that, regardless of the finlet spacing, a boundary layer separation sets in,

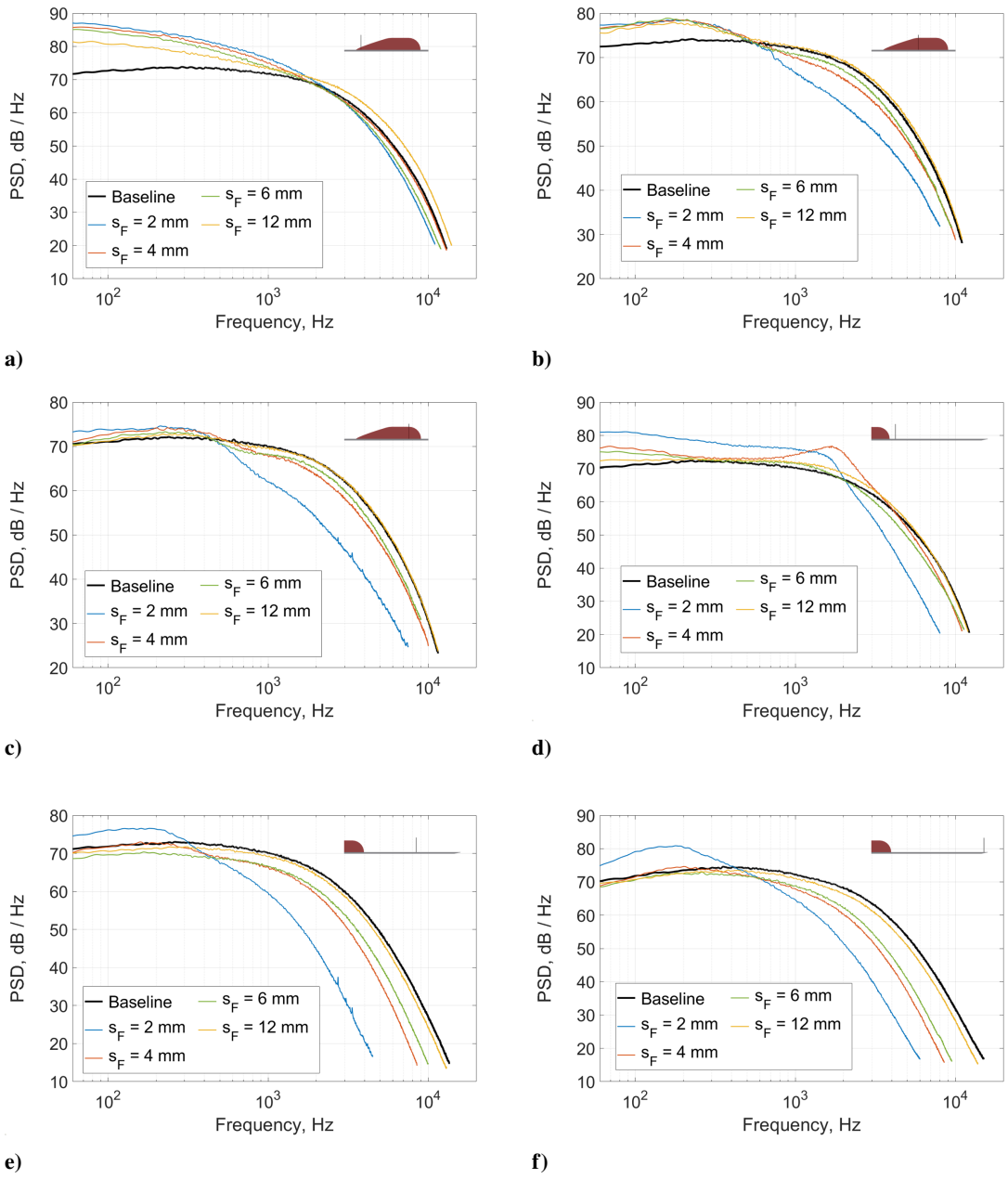

Fig. 6 Surface pressure fluctuation PSD for conventional finlets with $p_F = 0.835 \cdot L$, $h_F = 12\,\text{mm}$, $l_F = 65\,\text{mm}$ and various spacings at $Re_L = 9.9 \cdot 10^5$: a) $x/L = 0.84$, b) $x/L = 0.87$, c) $x/L = 0.888$, d) $x/L = 0.906$, e) $x/L = 0.954$ and f) $x/L = 0.996$.

which possibly causes an area of recirculation. Figures 6b and c describe the further development of the boundary layer within the finlets. The low-frequency elevations decrease quickly and Φ_{pp} is reduced at frequencies higher than 700 Hz for all treatments, except for the extreme case of $s_F = 12\,\text{mm}$. The treatment with the largest spacing seems to loose its capability to reduce the high-frequency pressure fluctuations due to the large distance between the finlet walls and the related data almost completely matches the baseline. An interesting situation arises directly at the finlet exit, as illustrated by Fig. 6d. The treatments with $s_F \geq 6\,\text{mm}$ show a decline of the low-frequency peak, whereas it grows again for $s_F = 2\,\text{mm}$. As discussed earlier, this could be an indicator for a recirculation bubble at the end of the

treatment, just as it would occur in the case of a backward facing step. The shape of the PSD curve for the treatment with $s_F = 4\,\text{mm}$ at this position shows a high similarity to the power spectrum for surface-pressure fluctuations measured by Cherry et al. [18] somewhat after flow reattachment studying a separated and reattaching flow. Thus, it can be deduced that the flow, separated at the front of the finlets, is likely to have reattached just about at their end for this particular treatment. With the turbulence being convected further toward the trailing edge and thus away from the treatment, the low-frequency peak disappeared for the finlets with $s_F \geq 4\,\text{mm}$, as can be seen in Figs. 6e and f. From these observations it can be inferred that the flow separation, in case the $s_F = 4\,\text{mm}$ - treatment is applied, is likely to extend only for a small distance in the wall-normal (i.e. y-) direction, such that a large portion of the turbulence is still forced through the gap between the finlets and thus channeled. Some of the small structures associated with the high-frequency pressure fluctuations seem to lose energy within the finlets, probably due to dissipation caused by the enlarged wetted surface area. However, the majority of the reduction took place in the finlet wake. It is assumed that the dissipation effect originating close to the finlet walls needs a development length and time to settle and take effects through the entire channeled flow, and into the wake of the finlets. By contrast, the low-frequency hump remains preserved across the entire range between the treatment and the trailing edge for $s_F = 2\,\text{mm}$. According to Afshari et al. [9], the hump resulted from a shear layer emerging on top of the treatment. The capability of such dense treatments to reduce Φ_{pp} at frequencies higher than 400 Hz at the trailing edge could be explained by the lifting effect mentioned by Bodling and Sharma [11, 12]. Small turbulent structures are likely to detach from the surface, deflected by the large structures arising at the finlet front. This turbulence then might remain attached, not interfering with the trailing edge when convected past it. Consistent with the results of Afshari et al. [9], the presented data definitely reveal two different noise reduction mechanisms induced by the presence of surface treatments. An increase at low frequencies up to 400 Hz and a strong decrease at higher frequencies was attributed to the pairing of small-scale eddies in the shear layer that formed at the ridges of the finlets, resulting in larger turbulence structures. This can be observed for treatments with small finlet spacing s_F, in the present study for the treatment with $s_F = 2\,\text{mm}$. With regard to the results presented in this investigation, it is postulated that there exists a region of detached flow in the area of the finlet leading edge, growing with decreasing s_F. For $s_F = 2\,\text{mm}$, the treatment is likely to be dense enough to generate a recirculation bubble that changes the flow physics permanently, leading to larger turbulence structures within the boundary layer and a decrease of small-scale eddies near the flat plate surface at the same time. For the cases, in which the surface pressure fluctuation PSD at the trailing edge remained lower than for the baseline across the entire frequency range, the flow is assumed to be channeled, where the turbulent structures pass through the gaps between the finlet walls instead of being deflected to travel along the finlet ridges. In this study, spacings of $s_F \geq 4\,\text{mm}$ seemed to result in channeling.

According to Amiet's theory, the magnitude of trailing-edge noise is predicated on both the surface pressure fluctuations analyzed above, and the spanwise correlation length of the boundary layer turbulence structures, Λ_z. Subsequently, Fig. 7 shows Λ_z as a function of frequency for finlet treatments with different spacings. The results again show a notable increase of the correlation length at frequencies below 500 Hz for the treated flat plate compared to the baseline. This suggests that the presence of finlets upstream of the trailing edge did not reduce noise through decreasing the correlation length of the turbulent structures within the boundary layer. Moreover, any reduction in the surface pressure fluctuations at relatively low frequencies will suffer a counter effect from the increase in correlation length. However, a large noise reduction potential can still be observed over a wide range of frequencies, where the reduction of Φ_{pp} approaches 10 dB to 20 dB with only slight increase in the spanwise correlation length.

Essential information on the effects the surface treatments have on the flow physics can be obtained from the velocity distribution in the boundary layer. The velocity profiles for finlet treatments with the same spacing applied at the same Reynolds number will depend on the measurement position relative to the treated area. However, the surface pressure fluctuation PSD discussed in Section IV.A suggest that the position ideal for trailing edge noise reduction lies near $p_F = 0.835 \cdot L$. Therefore, it seems obvious that for velocity measurements at the trailing edge, the finlets considered in this section provide the most relevant configuration for the investigation of the prevailing noise reduction mechanism. Moreover, it is assumed that the influence of the profile shape on the boundary layer velocity profile at the trailing edge is small for the considered application position, as it is likely that the profile shape only affects the flow in close proximity to the treatment. Thus, it is meaningful to present the quantities related to the boundary layer velocity in the context of an examination of the effects of finlet spacing. The boundary layer velocity profiles u/U_∞ for treatments with different s_F at $Re_L = 1.3 \cdot 10^6$ are depicted in Fig. 8. To obtain a general picture, the wall distance, y, was normalized with the boundary layer thickness of the baseline, δ, and the streamwise velocity, u, with the free stream velocity, U_∞. The boundary layer thickness was determined as the wall distance where u reached an absolute value of $0.99 \cdot U_\infty$. A clear trend can be observed for the treated configurations as s_F increases from 2 mm to 6 mm. Close to the flat plate's surface, the finlets caused a significant reduction of the streamwise velocity component u. Whereas for the baseline case

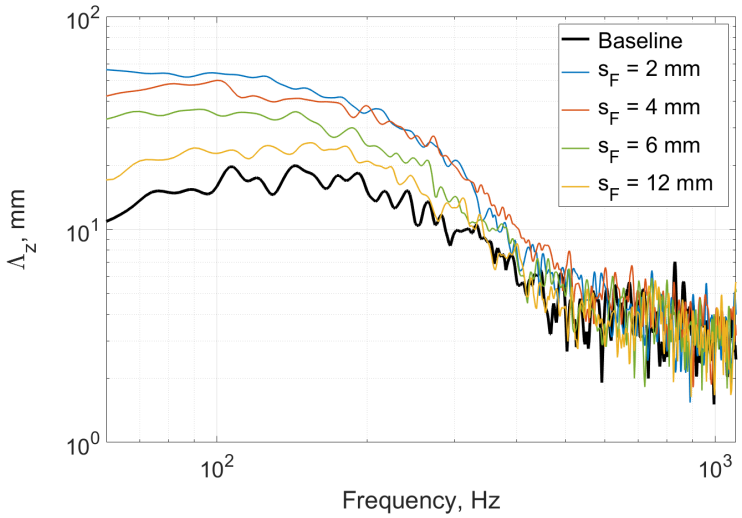

Fig. 7 Spanwise correlation length of the boundary layer turbulence structures at $x/L = 0.984$ for conventional finlets with $p_F = 0.835 \cdot L$, $h_F = 12\,\text{mm}$, $l_F = 65\,\text{mm}$, and various spacings at $Re_L = 9.9 \cdot 10^5$.

the velocity shows the usual logarithmic profile, a nearly linear growth of u can be observed for the treated flat plate. With a smaller spacing, the linear trend sets in earlier and the gradient gets steeper. At the transition to the free stream, the various profiles collapse quickly, without showing any signs of a velocity overshoot. The velocity decrease near the wall and the linear gradient indicate that viscous effects became more dominant across the boundary layer. Since the profiles show no overshoot, it can be assumed that for each case, turbulent structures were not just lifted but lost a portion of their kinetic energy due to viscous friction. For $s_F = 2\,\text{mm}$, the intersection point with the profile with $s_F = 4\,\text{mm}$ in the linear region at $y/\delta \approx 0.6$ suggests that a part of the flow was shifted away from the surface for the denser treatment. This agrees well with the earlier assumptions that if s_F falls below a certain threshold, turbulence is lifted away from the surface of the flat plate.

In order to examine the energy content of the turbulent boundary layer for the distinct treatments, the root-mean-square of the velocity fluctuations, u_{rms}, is investigated in the following, which will provide further insights into the flow characteristics. Since the velocity measurements were carried out using a single wire sensor probe, the turbulence contents are represented using u_{rms} instead of the squared quantities. As the fluctuations in the wall-normal and spanwise direction are much less significant as compared to the streamwise quantities, u_{rms} provides a satisfactory indicator to the flow turbulence within the boundary layer. Figure 9 shows the root-mean-square velocity profile u_{rms}/U_∞ for the finlets also considered in the investigation of the velocity profile at $Re_L = 1.3 \cdot 10^6$. To highlight the different noise reduction mechanisms, the wall distance was normalized by the finlet height. In doing so, it can be observed that for $s_F = 2\,\text{mm}$, the energy content shows a well-pronounced maximum at $y/h_F \approx 1$. This clearly indicates that turbulence was lifted away from the wall, concentrating at the finlet ridges. The other treatments also show a local extremum at this position. However, velocity fluctuations were still more intense near the wall, and the local extreme values of u_{rms} near $y/h_F = 1$ are lower. The two treatments with a wider spacing clearly show an overall reduction of kinetic energy, probably due to dissipation at the finlet walls. In the case of the treatments with $s_F = 2\,\text{mm}$ on the other hand, the kinetic energy did not seem to be dissipated. Instead, the energy content was rather relocated toward the finlet ridge, which was likely to result in a shear layer on top of the treatment as described by Afshari et al. [9]. However, the decrease of the kinetic energy close to the flat plate surface indicates a lack of the presence of small-scale eddies in this region and thus reinforces the argument that dense finlet treatments are capable to reduce trailing edge noise at high frequencies.

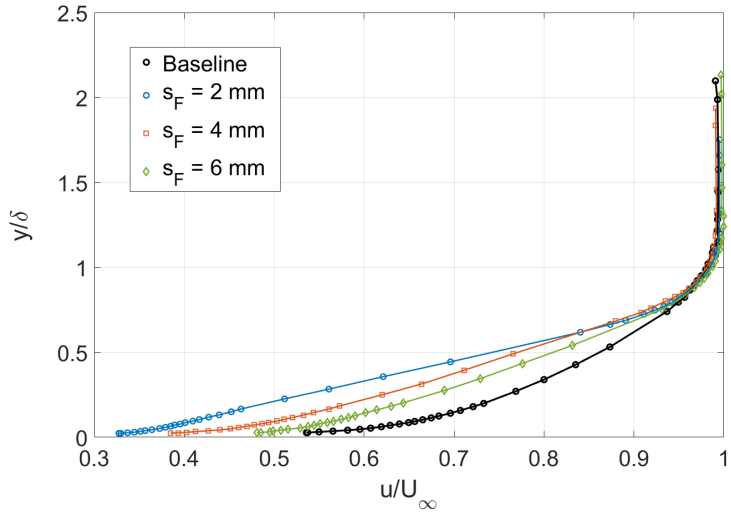

Fig. 8 Velocity profile u/U_∞ at $x/L = 0.996$ for conventional finlets with $p_F = 0.835 \cdot L$, $h_F = 12\,\text{mm}$, $l_F = 65\,\text{mm}$, and various spacings at $Re_L = 1.3 \cdot 10^6$.

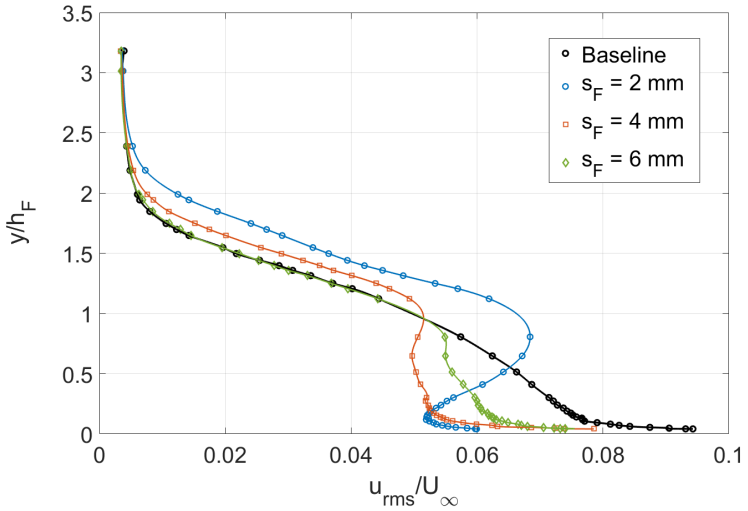

Fig. 9 Root-mean-square velocity profile u_{rms}/U_∞ at $x/L = 0.996$ for conventional finlets with $p_F = 0.835 \cdot L$, $h_F = 12\,\text{mm}$, $l_F = 65\,\text{mm}$, and different spacings at $Re_L = 1.3 \cdot 10^6$.

C. Effect of Finlet Profile Shape

The original finlet design was inspired from the downy structures of owl plumage. As observed by Clark et al. [5], these plumage structures protrude from the surface as arched profiles forming canopies. The arch was assumed to help avoid sudden changes to the boundary layer characteristics. Afshari et al. [8, 9] reconstructed them using a boundary layer profile approach, which was applied in this study as well. To understand the effects of different profile shapes, a simple, rectangular finlet profile was used as a contrast to the conventional ones, i.e. the ones used primarily in [9] and in the present study. Apart from the profile shape, the investigated finlet type is similar to the conventional treatment of height $h_F = 12\,\text{mm}$, spacing $s_F = 4\,\text{mm}$ and length $l_F = 65\,\text{mm}$ applied at the position $p_F = 0.835 \cdot L$. A comparison of the static pressure distributions for the different profile shapes at $Re_L = 1.3 \cdot 10^6$ is shown in Fig. 10. Following the streamwise development of the static pressure along the flat plate, a few important differences can be observed. First, the pressure upstream of the rectangular finlet treatment rose earlier and showed stronger fluctuations. The non-smooth

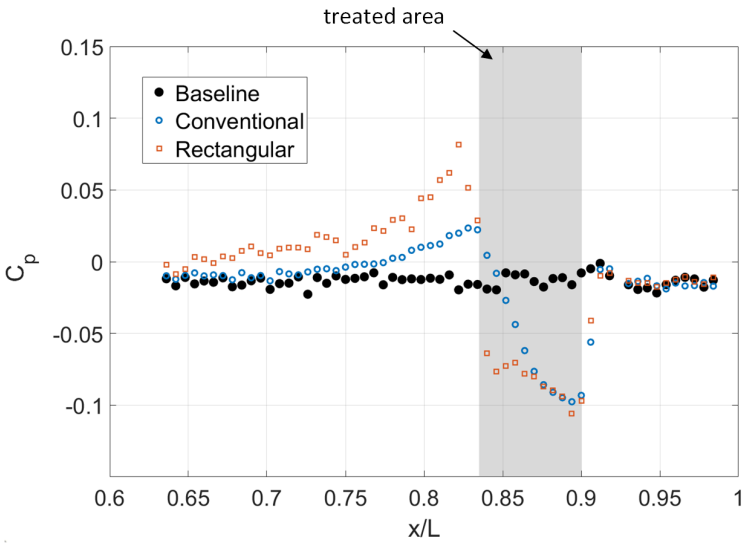

Fig. 10 Pressure coefficient for conventional and rectangular finlets with $p_F = 0.835 \cdot L$, $h_F = 12\,\text{mm}$, $l_F = 65\,\text{mm}$, and $s_F = 4\,\text{mm}$ at $Re_L = 9.9 \cdot 10^5$.

transition to a channel formed by the rectangular finlets seemed to affect the upstream flow in a harsher manner and is believed to possibly generate a higher drag. Within the treated area, the impact of the alternative profile shape was initially greater. The pressure drop sets in more abruptly, which probably reflects a stronger channeling effect for the rectangular profiles. After a short distance with a very strong favorable pressure gradient, the static pressure has a local minimum and subsequently rises constantly, and its gradient matches well with that of the conventional treatment. Just before the recovery region, the gradient increases one more time and the global minimum of the static pressure is reached. The recovery happened just as quickly as for the conventional finlets. The two minima at the front and the rear of the rectangular finlets were probably caused by the sudden contraction and expansion of the flow entering and leaving the treatment channels. It is thus assumed that the rectangular profile shape causes some pressure undershoots at the channel entrance and exit.

The results of the comparisons for both the surface pressure fluctuation PSD and spanwise correlation length are given in Figs. 11 and 12, respectively. The surface pressure fluctuation PSD for the two different finlet shapes are very similar. It can be seen from Figs. 11a to c that the application of rectangular finlets lead to an increase at the measurement positions inside the treated area at frequencies higher than 5000 Hz compared to the scenario with conventional finlets applied. At even higher frequencies, this rise in the PSD also exceeds the baseline. On the other hand, the application of rectangular finlets resulted in a clear reduction near the trailing edge at frequencies above 300 Hz with reference to the results for the conventional finlet treatment, as shown in Figs. 11d to f. Since the transitions from the "free" boundary layer to the treated area and the treated area to the wake were not as smooth as in the case of the conventional finlet treatment, the rectangular shape is prone to vibrations leading to an increase in the observed PSD. The tones, which can be observed in the depicted spectra at just above 2000 Hz, further indicate a flapping of the finlets subjected to airflow. Also, the extrema of the static pressure occurring near the finlet leading and trailing edges for the rectangular shape suggest that the flow is disturbed more drastically by the non-smooth edges of the rectangular finlet walls. Therefore, it is postulated that, due to the non-smooth leading and trailing edges, the rectangular finlet walls flutter in the air stream, causing tones and high-frequency pressure fluctuations. From the lack of a significant low-frequency peak of the surface pressure fluctuation PSD at the trailing edge, it can be inferred that the turbulence was also channeled and thus convected mainly through the gaps between the finlets. The reduced surface pressure fluctuation PSD downstream of the finlets near the trailing edge reinforce the argument of a stronger channeling effect induced by the rectangular profile shape. As it is assumed that the spanwise length scale is mainly influenced by a change of spanwise treatment characteristics, it is not surprising that the results for Λ_z seem to be independent of the profile shape when the finlet spacing is unchanged.

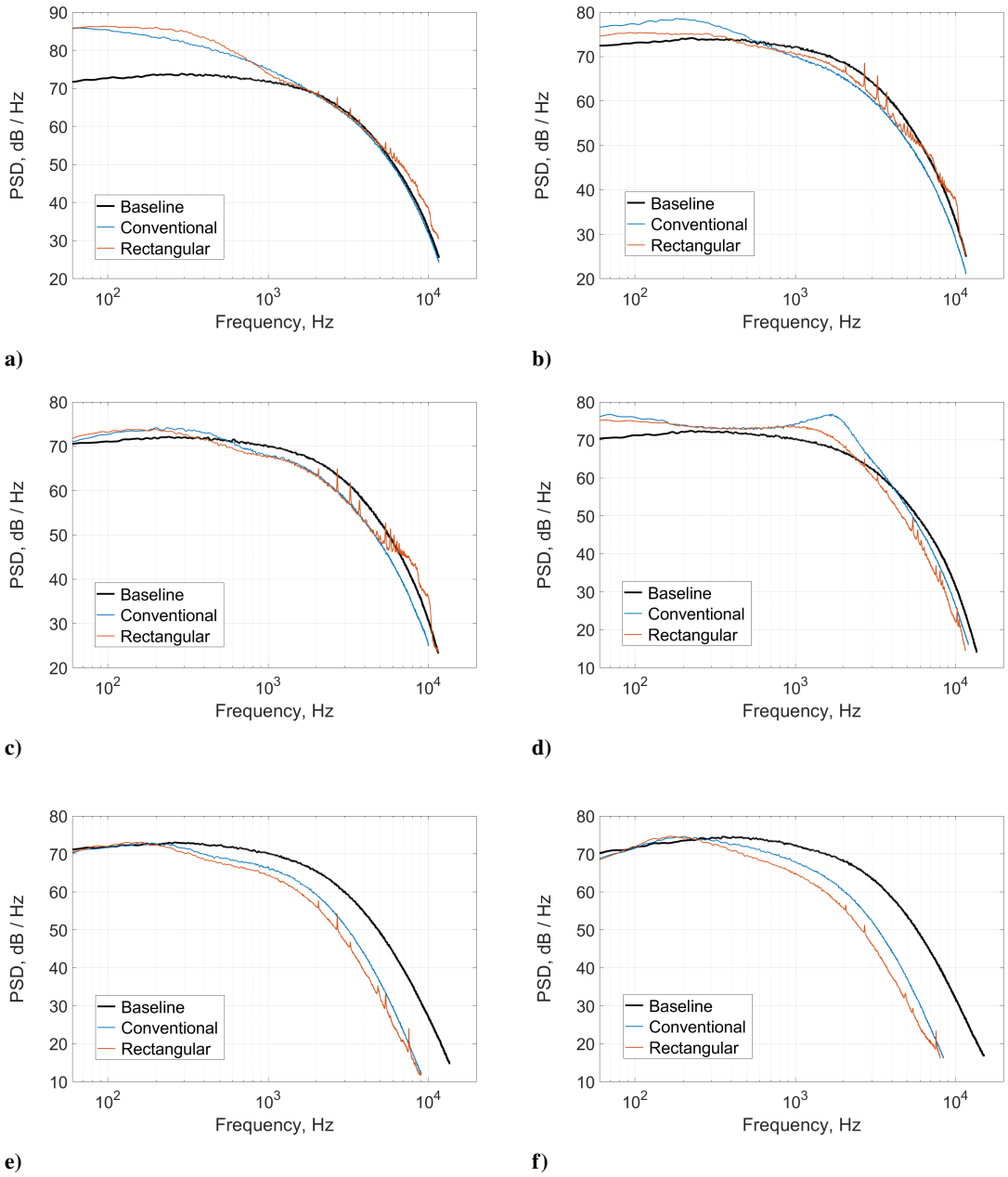

Fig. 11 Surface pressure fluctuation PSD for conventional and rectangular finlets with $p_F = 0.835 \cdot L$, $h_F = 12\,\text{mm}$, $l_F = 65\,\text{mm}$ and $s_F = 4\,\text{mm}$ at $Re_L = 9.9 \cdot 10^5$: a) $x/L = 0.84$, b) $x/L = 0.87$), c) $x/L = 0.888$, d) $x/L = 0.906$, e) $x/L = 0.954$ and f) $x/L = 0.996$.

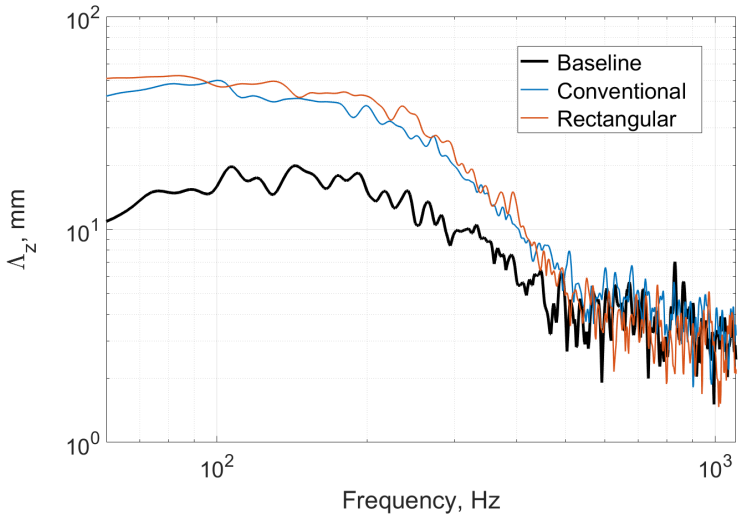

Fig. 12 Spanwise correlation length of the boundary layer turbulence structures at $x/L = 0.984$ for conventional and rectangular finlets with $p_F = 0.835 \cdot L$, $h_F = 12\,\text{mm}$, $l_F = 65\,\text{mm}$, and $s_F = 4\,\text{mm}$ at $Re_L = 9.9 \cdot 10^5$.

V. Conclusions and Future Work

A parametric study comprising different placement locations and spacings has been performed for a range of conventional finlet treatments in order to investigate their effects on the trailing edge noise. The design of the conventional finlets is similar to that proposed by Afshari et al. [8, 9]. The experimental set-up was carefully conceived to allow measurements of both the static and dynamic pressure to be performed in the gap between the finlets. This was done to reveal in more detail the underlying flow physics and its connection to trailing edge noise reduction. It has been demonstrated that, whereas the spanwise correlation length increases slightly, the surface pressure fluctuation PSD reduces much more pronouncedly when the finlet treatments are applied. This can be attributed to the channeling phenomenon and the subsequent reorganization of the turbulent structures within the boundary layer. Application of finlets further upstream of the trailing edge has shown to be more efficient in the overall reduction of Φ_{pp}, probably allowing the boundary layer to evolve and settle to a preferred state rather than being scattered immediately when leaving the finlets in a disturbed state. By comparison of the conventional with the rectangular finlet profiles, the consequences of a non-smooth transition to the treated area were demonstrated. The rectangular treatments are able to reduce the near-field surface pressure PSD even further than the conventional finlet treatments at the trailing edge. However, as a consequence of the non-smooth flow transitions at the leading and trailing edges of the finlets, the rectangular treatments showed tones, probably originating from a flapping motion of the finlet walls. These tones are likely to be radiated as far-field noise.

Acknowledgments

The first author appreciates the financial support of the EU H2020 ARTEM project under the grant agreement ID 769359, which made this work possible. The research process was also facilitated by Neil Pearce, who manufactured the flat plate, and Lee Winter, who spent hours of tedious work fitting brass tubes for the pressure taps. Special thanks also go to David Godoy Alonso for the design of new power boxes regulating the input voltage for the pressure transducers used during the experiments.

References

[1] Darecki, M., Edelstenne, C., Enders, T., Fernandez, E., Hartman, P., Herteman, J.-P., Kerkloh, M., King, I., Ky, P., Mathieu, M., Orsi, G., Schotman, G., Smith, C., and Wörner, J.-D., "Flightpath 2050 Europes Vision for Aviation," *Publications Office of the European Union*, 2011.

[2] Lockard, D. P., and Lilley, G. M., "The airframe noise reduction challenge," Tech. mem. tm–2004–213013, NASA, Langley Research Center, Hampton, Virginia, 2004.

[3] Amiet, R. K., "Noise due to turbulent flow past a trailing edge," *Journal of Sound and Vibration*, Vol. 47, No. 3, 1976, pp. 387–393.

[4] Lilley, G. M., "A study of the silent flight of the owl," *4th AIAA/CEAS Aeroacoustics Conference*, 1998.

[5] Clark, I. A., Devenport, W., Jaworski, J. W., Daly, C., Peake, N., and Glegg, S., "The noise generating and suppressing characteristics of bio-inspired rough surfaces," *20th AIAA/CEAS Aeroacoustics Conference*, 2014.

[6] Clark, I. A., Baker, D., Alexander, W. N., Devenport, W., Peake, N., Glegg, S., and Jaworski, J. W., "Experimental and theoretical analysis of bio-inspired trailing edge noise control devices," *22nd AIAA/CEAS Aeroacoustics Conference*, 2016.

[7] Clark, I. A., Alexander, W. N., Devenport, W., Glegg, S., Jaworski, J. W., Daly, C., and Peake, N., "Bioinspired trailing-edge noise control," *AIAA Journal*, Vol. 55, No. 3, 2017, pp. 740–754.

[8] Afshari, A., Azarpeyvand, M., Dehghan, A. A., and Szőke, M., "Effects of streamwise surface treatments on trailing edge noise reduction," *23rd AIAA/CEAS Aeroacoustics Conference*, 2017.

[9] Afshari, A., Azarpeyvand, M., Dehghan, A. A., Szöke, M., and Maryami, R., "Trailing-edge flow manipulation using streamwise finlets," *Journal of Fluid Mechanics*, Vol. 870, 2019, pp. 617–650.

[10] Afshari, A., Dehghan, A. A., and Azarpeyvand, M., "Novel three-dimensional surface treatments for trailing-edge noise reduction," *AIAA Journal*, Vol. 57, No. 10, 2019, pp. 4527–4535.

[11] Bodling, A., and Sharma, A., "Numerical investigation of low-noise airfoils inspired by the down coat of owls," *Bioinspiration and Biomimetics*, Vol. 14, No. 1, 2019.

[12] Bodling, A., and Sharma, A., "Numerical investigation of noise reduction mechanisms in a bio-inspired airfoil," *Journal of Sound and Vibration*, Vol. 453, 2019, pp. 314–327.

[13] Gravante, S. P., Naguib, A. M., Wark, C. E., and Nagib, H. M., "Characterization of the pressure fluctuations under a fully developed turbulent boundary layer," *AIAA Journal*, Vol. 36, No. 10, 1998, pp. 1808–1816.

[14] Mayer, Y. D., Jawahar, H. K., Szőke, M., Ali, S. A. S., and Azarpeyvand, M., "Design and performance of an aeroacoustic wind tunnel facility at the University of Bristol," *Applied Acoustics*, Vol. 155, 2019, pp. 358–370.

[15] Garcia-Sagrado, A., and Hynes, T., "Wall pressure sources near an airfoil trailing edge under turbulent boundary layers," *Journal of Fluids and Structures*, Vol. 30, 2012, pp. 3–34.

[16] Ali, S. A. S., Azarpeyvand, M., and Da Silva, C. R. I., "Trailing-edge flow and noise control using porous treatments," *Journal of Fluid Mechanics*, Vol. 850, 2018, pp. 83–119.

[17] Szoke, M., Fiscaletti, D., and Azarpeyvand, M., "Effect of inclined transverse jets on trailing-edge noise generation," *Physics of Fluids*, Vol. 30, No. 8, 2018.

[18] Cherry, N. J., Hillier, R., and Latour, M. E., "Unsteady measurements in a separated and reattaching flow," *Journal of Fluid Mechanics*, Vol. 144, 1984, pp. 13–46.